An MC-SCF Study of the (Photochemical) Paterno–Buchi Reaction

Ian J. Palmer,‡ Ioannis N. Ragazos,‡ Fernando Bernardi,*,† Massimo Olivucci,† and Michael A. Robb*,‡

Contribution from the Dipartimento di Chimica "G. Ciamician" dell'Universita di Bologna, Via Selmi 2, 40126 Bologna, Italy, and the Department of Chemistry, King's College, London, Strand, London WC2R 2LS, U.K.

*Received September 16, 1992. Revised Manuscript Received November 8, 1993**

Abstract: An MC-SCF/6-31G* study of the singlet and triplet Paterno–Buchi reaction (for the model system formaldehyde and ethylene) is presented. In addition to the computation of the relevant minima and transition structures, the Born–Oppenheimer violation regions, where a fast decay from the singlet excited state (S_1) to the ground state (S_0) surface takes place, have been fully characterized by locating and optimizing the structure of two different S_0/S_1 conical intersections. The photochemical mechanisms of oxetane formation via carbon–carbon (C–C) and carbon–oxygen (C–O) attacks have both been investigated. For the C–C attack the singlet mechanism can be concerted as the decay to the ground state takes place in a point where the C–C bond is fully formed. Thus, starting from this decay point, the system can evolve directly to oxetane or produce a C–C bonded transient diradical intermediate. The C–O attack leads to a nonconcerted path only. In this case, the excited-state branch of the reaction coordinate terminates in a conical intersection point at a C–O distance of 1.77 Å before the diradical is fully formed. Thus, the system can evolve back to the reactant or produce a C–O bonded transient diradical intermediate that is isolated by very small barriers to fragmentation or ring-closure to oxetane. While the diradical structures corresponding to the two modes of attack differ in energy by only 8 kcal mol^{-1}, the S_1 to S_0 decay point for C–C attack lies 33 kcal mol^{-1} below the corresponding point for C–O attack. The triplet diradicals have energies and geometries that are very similar to the singlets. Thus we predict that intersystem crossing from triplet to singlet will lead to the same diradical ground-state pathways that can be entered via singlet photochemistry.

1. Introduction

The formation of oxetanes via the photochemical addition of carbonyl compounds to alkenes—the Paterno–Buchi reaction—was first reported in 1909.[1] It has been extensively investigated from a mechanistic point of view.[2–8] The reaction is of considerable importance in synthetic applications, and its utility has been documented in two comprehensive review articles.[7,8] The simplest model system for this reaction (Scheme 1) is the addition of formaldehyde (**1**) and ethylene (**2**) to form the parent oxetane (**4**) and is the subject of the computations reported in this work. From a formal point of view, the reaction is usually assumed to take place from reaction of $^{1,3}(n\text{-}\pi^*)$ formaldehyde with ground-state ethylene via the initial formation of 1,4-diradicals[4c] resulting from C–O attack (**3a**) or C–C attack (**3b**). However, such a scheme makes no reference as to whether these 1,4-diradicals are real intermediates. The electronic aspects of the Paterno–Buchi reaction were discussed many years ago by Zimmerman[5] who first proposed the involvement of 1,4-diradicals. He suggested[5] that during the attack of the electron-deficient p_y orbital of the $^{1,3}(n\text{-}\pi^*)$ formaldehyde on π systems, the product formed is controlled by a preference for the most stable 1,4-diradical. The mechanistic consequences of C–O versus C–C attack via the involvement of 1,4-diradicals remains the subject of current work from the Zimmerman group.[6] While the basic features of a mechanism involving 1,4-diradicals are well established in the literature, there has never been a systematic investigation of what part of the reaction path in Scheme 1 lies on the ground state and which part lies on the excited state.

Scheme 1

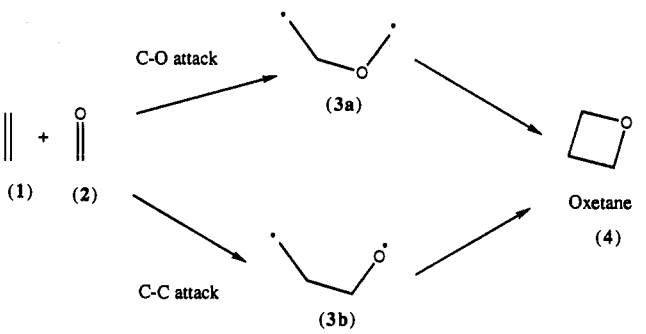

In order to understand the nonadiabatic nature of the reaction paths one needs to discuss the electronic configurations of he diradicals **3a** and **3b**. Accordingly, in Figure 1 (**I–IV**) we illustrate the four possible electronic configurations (VB structures) for the diradicals resulting from carbox–oxygen (**I–II**) or carbon–carbon (**III–IV**) bond formation. In VB structures **I** and **II**, an electron on the carbonyl oxygen and an electron on an alkene carbon are spin coupled to form a carbon–oxygen bond. The orientation of the remaining orbitals representing the diradical centers in diradical **I** clearly indicates an *electronic* correlation with the ground-state configuration at reactants (or products) and this is reflected in the parallel nature of the fragments in the diradical geometry. Thus as the C–O σ-bond breaks, the electrons recouple to form a C–O π bond and a C–C π bond. Diradical **II**, however, correlates electronically with an $n\text{-}\pi^*$ excited-state

† Dipartimento Chimico "G. Ciamician" dell'Universita di Bologna.
‡ Chemistry Department, King's College London.
* Abstract published in *Advance ACS Abstracts*, January 15, 1994.

(1) Paterno, E.; Chiefi, G. *Gazz. Chim. Ital.* **1909**, *39*, 431.
(2) (a) Buchi, G.; Inman, C. G.; Lipinsky, E. S. *J. Am. Chem. Soc.* **1954**, *76*, 4327. (b) Buchi, G.; Kofron, J. T.; Koller, E.; Rosenthal, D. *J. Am. Chem. Soc.* **1956**, *78*, 876.
(3) Dalton, J. C.; Turro, N. J. *Ann. Rev. Phys. Chem.* **1970**, *21*, 499.
(4) (a) Turro, N. J. *Pure Appl. Chem.* **1971**, *27*, 679. (b) Turro, N. J.; Dalton, J. C.; Dawes, K.; Farrington, G.; Hautala, R.; Morton, D.; Niemczyk, M.; Schore, N. *Acc. Chem. Res.* **1972**, *5*, 92. (c) Turro, N. J. *Modern Molecular Photochemistry*; Benjamin/Cummings: 1978; p 432.
(5) Zimmerman, H. *Science* **1966**, *153*, 837.
(6) Zimmerman, H.; Wright, C. W. *J. Am. Chem. Soc.* **1992**, *114*, 363.
(7) Arnold, D. R. *Adv. Photochem.* **1968**, *6*, 301.
(8) Jones II, G. *Org. Photochem.* **1981**, *5*, 1.

0002-7863/94/1516-2121$04.50/0

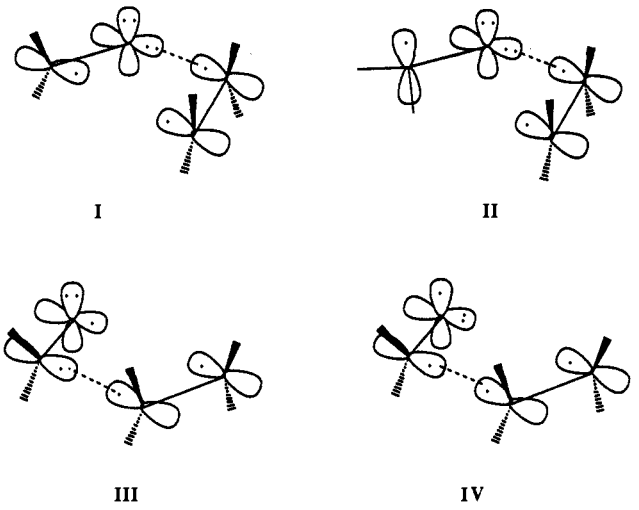

Figure 1. Valence bond (VB) resonance structures for 1,4-diradical geometries for C–O (I + II) and C–C (III + IV) mechanisms.

C–O and a ground-state ethylene and has the carbonyl and alkene fragments mutually perpendicular in the diradical geometry. Consequently, for the C–O bonded diradical it is possible to change diabatic surfaces (i.e., electronic configuration) via a simple *geometric* rotation of the terminal methyl group. While the initial stage of the photochemical reaction (n-π^* excited state C–O) will involve the formation of diradical **II** this diradical cannot close to the oxetane product without rotation of the terminal methyl group. Thus, it is diradical **I** that correlates with the product oxetane.

The C–C diradicals, **III** and **IV**, have an electron on the carbonyl carbon spin coupled with one of the electrons of the alkene π system resulting in the formation of a C–C bond. Once this bond has completely formed, one electron on the O atom of the formaldehyde and the remaining electron the C atom of the ethylene are completely "decoupled" yielding a true diradical. The unpaired electron on the O atom of the formaldehyde can be in either a p^π orbital to give diradical **III** or an *n* orbital to give diradical **IV**. Diradical **III**, according to the configuration of the electrons in the oxygen orbitals, correlates electronically with ground-state reactants. Diradical **IV** correlates electronically with an n-π^* excited-state C–O and a ground-state C=C. Thus for the C–C mechanism it is possible to change between diabatic surfaces via an *orbital* rotation at the oxygen center in contrast to the C–O mechanism where a *geometric* rotation is necessary. Like the C–O diradical, the initial stage of the photochemical reaction (n-π^* excited state C–O) will involve the formation of diradical **IV**, and this diradical cannot close to the oxetane product which must occur from diradical **III**.

The preceding discussion indicates that the Paterno–Buchi reaction must be nonadiabetic. The reaction starts on a excited-state potential surface and must yield diradicals **II** or **IV**. The final stage of the reaction must proceed to a bonding ground-state configuration from diradicals **I** or **III**. The decay from the excited state (S_1) to ground state (S_0) must occur via a Born–Oppenheimer violation (i.e., a surface *hop*) for the singlet reaction and via intersystem crossing for the triple reaction. For most photoreactions, it is still largely unknown at what point along the reaction coordinate the photoexcited reactants relax (the reaction "funnel" [9-14]. Zimmerman (see ref 9a, footnote 8b) has recognized the fundamental role of the reaction "funnel" in 1966. Thus the characterization of a photochemical reaction involves, in addition to the usual study of ground- and excited-state reaction paths, a characterization of the region where Born–Oppenheimer violation or singlet–triplet crossing occurs, and the system decays nonradiatively to S_0.

Recent work has provided evidence for the involvement of conical intersections[14-19] in the mechanisms of singlet photochemical reactions of organic[20] and inorganic[21] systems. At a conical intersection point, one has an ultrafast decay (within a vibrational period[22]) from the upper to the lower potential energy surface, and thus a fully efficient radiationless relaxation mechanism for the photoexcited reactant. Consequently, the rigorous location and characterization of conical intersections is of central importance in the study of photochemical mechanisms. For the system under investigation, we will demonstrate that there are two conical intersection points located near the C–C and C–O bonded diradical regions of the ground state. These two conical intersections support a mechanism where the decay from the excited state is accompanied by a *geometric* rotation of the terminal methyl group, in the case of C–O attack, and by an *orbital* rotation at the oxygen center, in the case of C–C attack. Thus the central feature of the mechanism occurs at the C–O and C–C conical intersections where the configuration of diradical **II** is converted to that of diradical **I** and the configuration of diradical **IV** is converted to that of **III**.

Experimental evidence[23-27] supports the role of diradicals as one of the central features in the mechanism and the actual detection of transient triplet diradical species has been made using picosecond absorption techniques.[26] Although, the mechanism is often assumed to involve the C–O attack, Turro[4c] has suggested on the basis of orbital correlation diagrams that both mechanisms may operate. Indeed there is no experimental evidence that contradicts the conjecture that both mechanisms may operate. C–C attack is often postulated in the intramolecular interaction of a C=O with a C=C system in the oxy-di-π-methane rearrangement. In recent work Zimmerman[6] has also studied the rearrangement of acylcyclopropenes to furans. In this work he considers both C–C attack and C–O attack and gives convincing evidence that C–O attack dominates in this case. However this could be simply a result of steric effects since the intermediate 1,4-diradical for C–O attack involves the formation of a three-membered ring, while C–O attack generates a four-membered

(9) (a) Zimmermann, H. E. *J. Am. Chem. Soc.* **1966**, *88*, 1566. (b) Zimmermann, H. E. *Acc. Chem. Res.* **1972**, *5*, 393. (c) Zimmermann, H. E.; Factor, R. E. *J. Am. Chem. Soc.* **1980**, *102*, 3538.

(10) Michl, J.; Bonacic-Koutecky, V. *Electronic Aspects of Organic Photochemistry*; Wiley: 1991; p 397.

(11) Van der Lugt, W. T. A. M.; Oesteroff, L. J. *J. Am. Chem. Soc.* **1969**, *91*, 6042.

(12) Gimbert, D.; Segal, G.; Devaquet, A. *J. Am. Chem. Soc.* **1975**, *97*, 6629.

(13) Bonacic-Koutecky, V.; Michl, *J. Angew. Chem., Int. Ed. Engl.* **1987**, *26*, 170.

(14) Salem, L. *Electrons in Chemical Reactions: First Principles*; Wiley: New York, 1982.

(15) Von Neumann, J.; Wigner, E. *Physik. Z.* **1929**, *30*, 467.

(16) Teller, E. *J. Phys. Chem.* **1937**, *41*, 109.

(17) Herzberg, G.; Longuet-Higgins, H. C. *Trans. Faraday Soc.* **1963**, *35*, 77.

(18) Ragazos, I. N.; Robb, M. A.; Olivucci, M.; Bernardi, F. *Chem. Phys. Lett.* **1992**, *197*, 217.

(19) Xantheas, S.; Elbert, S. T.; Ruegenberg, K. *J. Chem. Phys.* **1990**, *93*, 7519.

(20) (a) Bernardi, F.; De, S.; Olivucci, M.; Robb, M. A. *J. Am. Chem. Soc.* **1990**, *112*, 1737–1744. (b) Bernardi, F.; Olivucci, M.; Robb, M. A. *Acc. Chem. Res.* **1990**, *23*, 405–412. (c) Bernardi, F.; Olivucci, M.; Ragazos, I. N.; Robb, M. A. *J. Am. Chem. Soc.* **1992**, *114*, 2752–2754. (d) Bernardi, F.; Olivucci, M.; Robb, M. A.; Tonachini, G. *J. Am. Chem. Soc.* **1992**, *114*, 5805–5812. (e) Bernardi, F.; Olivucci, M.; Ragazos, I. N.; Robb, M. A. *J. Am. Chem. Soc.* **1992**, *114*, 8211–8220. (f) Palmer, I.; Bernardi, F.; Olivucci, M.; Robb, M. A. *J. Org. Chem.* **1992**, *57*, 5081–5087. (g) Domke, W.; Sobolewski, A. L.; Woywod, C. *Chem. Phys. Lett.* **1993**, *203*, 220.

(21) (a) Atchity, G. J.; Xantheas, S. S.; Elbert, S. T.; Ruedenberg, K. *J. Chem. Phys.* **1991**, *94*, 8054–8069. (b) Atchity, G. J.; Xantheas, S. S.; Elbert, S. T.; Ruedenberg, K. *Theor. Chim. Acta* **1991**, *78*, 365. (c) Muller, H.; Koppel, H.; Cederbaum, L. S.; Schmelz, T.; Chambaud, G.; Rosmus, P. *Chem. Phys. Lett.* **1992**, *197*, 599–606. (d) Manaa, M. R.; Yarkony, D. R. *J. Chem. Phys.* **1990**, *93*, 4473. (e) Manaa, M. R.; Yarkony, D. R. *J. Chem. Phys.* **1992**, *97*, 715–717.

(22) Manthe, U.; Koppel, H. *J. Chem. Phys.* **1990**, *93*, 1669.

(23) Carless, H. A. J. *J. Chem. Soc., Perkin Trans. II* **1974**, 834.

(24) Shimizu, N., et al. *J. Am. Chem. Soc.* **1974**, *96*, 6456.

(25) Yang, N. C., et al. *Tetrahedron Lett.* **1964**, 3657.

(26) (a) Freilich, S. C.; Peters, K. S. *J. Am. Chem. Soc.* **1981**, *103*, 6255. (b) Freilich, S. C.; Peters, K. S. *J. Am. Chem. Soc.* **1985**, *107*, 3819.

(27) Timpe, H. J.; Kronfeld, K. P.; Schiller, M. *J. Photochem. Photobiol. A: Chem.* **1991**, *62*, 245.

Scheme 2

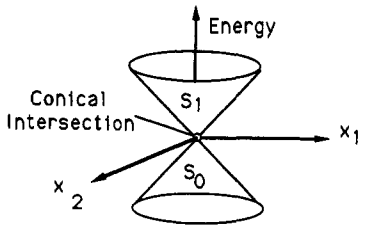

ring. While a few theoretical results[28-32] are available, only in the work of Salem[30] is the nonadiabatic nature of the reaction recognized.

In this paper we will try to gain an understanding of the photochemical mechanism of the Paterno–Buchi reaction through a study of the model formaldehyde/ethylene system (Scheme 1). While a reaction path involving the formation of ground-state 1,4-diradicals is accepted as the mechanism, the way in which these structures are formed after photoexcitation has never been established. Thus the location and characterization of the decay points where fast return to the ground state takes place is our central objective.

2. Methodological and Computational Details

All calculations have been performed using the implementation of the CASSCF procedure and standard 6-31G* basis set available in the Gaussian 91 package.[33] The CASSCF active space comprised six electrons distributed in five orbitals originating from the π and π^* orbitals of ethylene and the π, π^* and n orbitals of formaldehyde. The oxygen in the formaldehyde has two lone pairs, one is located in the 2s shell and the other in a "p"-like orbital which lies in the plane orthogonal to the p^π orbitals of the double bond. The lone pair active in the n–π^* electronic transition is the one located in the p-like orbital and so this was included in the active space. Geometry optimizations have been performed using analytic gradient techniques and critical points characterized via analytic second derivative calculations. All critical points have been converged to the default convergence of the Gaussian optimization algorithms (maximum force of 0.000 45 au) unless otherwise stated.

The rigorous location of low-lying conical intersection points[15-19] requires a nonstandard method[18] that has been implemented in a development version of the Gaussian package. For polyatomic systems the real crossing of two potential energy surfaces of the same spin multiplicity forms a *(n – 2)-dimensional hyperline* called the *intersection space*.[34] At any point on the *intersection space* one can identify two independent directions, say x_1 and x_2 that remove the degeneracy. If we plot the energy versus these two directions, the ground- and excited-state surfaces appear as a double-cone with the degeneracy located at the common apex of the two cones (see Scheme 2). Thus any point of the intersection space lies on the conical intersection. As we have discussed elsewhere[18] the directions x_1 and x_2 correspond to a vector parallel to the nonadiabatic coupling vector, $\langle\Psi_1|\partial\Psi_2/\partial\mathbf{q}\rangle$, and a vector parallel to gradient difference vector, $\partial(E_2 - E_1)/\partial q$ (where q is a nuclear displacement vector). Movement through geometries residing in the intersection space preserves the degeneracy. (For an early discussion of this point by Zimmerman in the context of MO theory see ref 9b.) The potential energy plotted along the intersection space will possess its own distinct topology of transition states and minima. As we will see below we are particularly interested in locating the lowest energy minimum on a given intersection space.

For triatomic systems the conical intersection line ($n - 2 = 1$) can be mapped out accurately.[19,21d,e] However these techniques need some modification for many degrees of freedom where the intersection space is a hyperline. However, the lowest energy point on the intersection space can be determined using standard methods, and we have described an algorithm in ref 18 that is an extension of the method used in ref 21d,e. One simply minimizes the energy in the $n - 2$ dimensional subspace subject to the constraint that the two states are degenerate. One can clearly distinguish the case of an avoided crossing (with a very small energy gap) with a true intersection because the gradient of the excited state vanishes in the former case but not the latter (where only the projection of the gradient in the $n - 2$ space is zero). The singlet/triplet crossing is similar except that the crossing surface is of dimension $n - 1$ as discussed recently by Yarkony.[35]

We are thus using a model where the S_1 to S_0 decay point (where a surface hop takes place) is a conical intersection. In particular we want to locate the minimum of a $n - 2$ dimensional S_1/S_0 intersection space, i.e., the lowest energy conical intersection point. This point provides the lowest energy decay point for the surface hop. Of course, a surface hop will have a high probability at all *energetically accessible points* on the intersection space. Nevertheless, in condensed phases, one assumes that one will follow a S_1 reaction coordinate that lies along the steepest descent pathways. Such pathways will terminate at low-energy points on the S_1/S_0 conical intersection hyperline.

In order to optimize conical intersection geometries, one needs to use state averaged MC-SCF.[21d,e] In this procedure, the orbitals are optimized for an average of the two states involved. Such a procedure is similar in spirit to the averaging over degenerate multiplets that is used in an SCF computation for an open shell atom or linear diatomic molecule. Because of this, the energies are not strictly comparable (i.e., they must be slightly higher) with the energies of other critical points determined.

3. Results and Discussion

The MC-SCF/6-31G* ground- and excited-state minima structures are displayed in Figure 2a–d. The energies of all of our computed structures are given in Table 1. The structural information for C–O attack (Scheme 1, **1** + **2** → **3a** → **4**) is given in Figures 3–6, while the corresponding data for C–C attack (Scheme 1, **1** + **2** → **3b** → **4**) is collected in Figures 7–9. The structures of the triplet 1,4-diradical minima are in Figure 10. The energies for the reference reactant ethylene–formaldehyde region of the potential surface are obtained via simple addition of the energies of the individual reactant molecules. Obviously, SCF is adequate for treating the ground state minima. However, in order to compare energies we must use MC-SCF even for the closed shell minima.

I. Singlet Carbon–Oxygen Reaction Path. The first mechanism to be discussed corresponds to an attack of the carbonyl oxygen on the ethylenic fragment (Scheme 1, **1** + **2** → **3a** → **4**) leading to the formation of a carbon–oxygen bond and a 1,4-diradical species with two carbon radical centers (Figure 1, **I** + **II**). On the ground state the carbonyl and ethylene will approach along a "parallel" coordinate, i.e., the π systems of the two fragments will lie in the same plane, whereas the reaction of the n-π^* excited formaldehyde will occur with the carbonyl fragment lying perpendicular to the ethylene to facilitate the attack of the half filled "n" orbital of the oxygen. Both a *gauche* and *trans* approach is possible.

(28) Herndon, W. C.; Giles, W. B. *Mol. Photochem.* **1970**, *2*, 277.
(29) Herndon, W. C. *Tetrahedron Lett.* **1971**, (*2*), 125.
(30) Salem, L. *J. Am. Chem. Soc.* **1974**, *96*, 3486.
(31) Arnaut, L. G.; Formosinho, S. J. *J. Photochem.* **1987**, *39*, 13.
(32) Chen, G.; Fang, D.; Fu, X. *Int. J. Quantum Chem. Symp.* **1989**, *23*, 501.
(33) *Gaussian 91 (Revision C)*; Frisch, M. J.; Head-Gordon, M.; Trucks, G. W.; Foresman, J. B.; Schlegel, H. B.; Raghavachari, K.; Robb, M.; Wong, M. W.; Replogle, E. S.; Binkley, J. S.; Gonzalez, C.; Defrees, D. J.; Fox, D. J.; Baker, J.; Martin, R. L.; Stewart, J. J. P.; Pople, J. A. Gaussian, Inc.: Pittsburgh, PA, 1991.
(34) Atchity, G. J.; Xantheas, S. S.; Ruegenberg, K. *J. Chem. Phys.* **1991**, *95*, 1862.
(35) Yarkony, D. R. *J. Am. Chem. Soc.* **1992**, *114*, 5406.

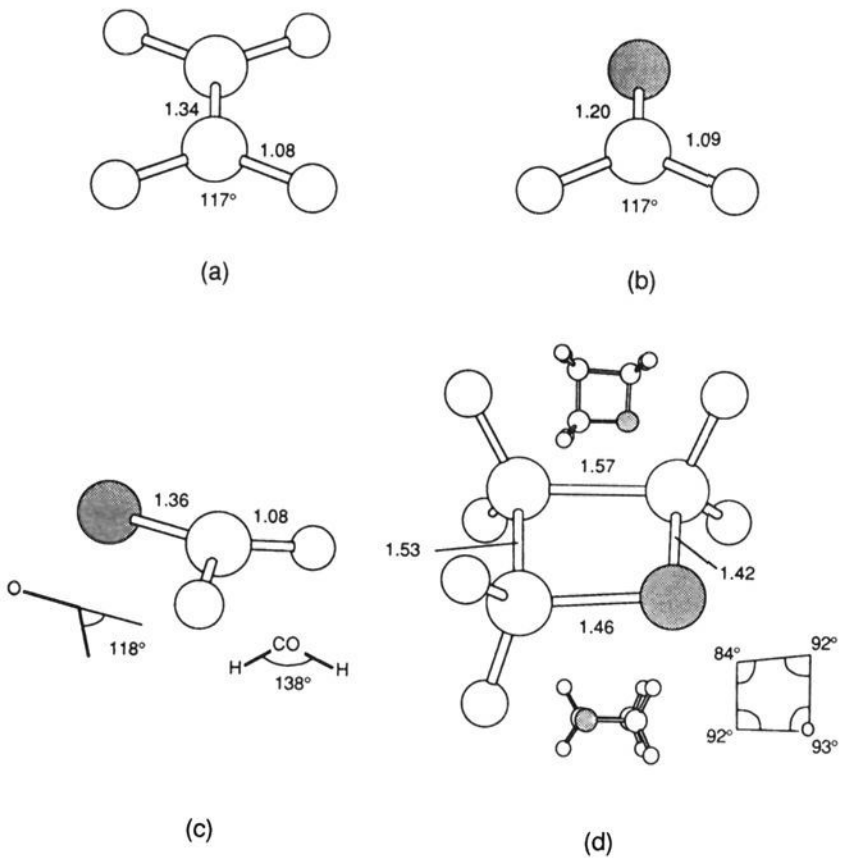

Figure 2. Optimized CASSCF/6-31G* geometries for (a) ground-state ethylene, (b) ground-state formaldehyde, (c) excited-state formaldehyde, and (d) ground-state oxetane (bond lengths are in Å and angles in deg).

The MC-SCF/6-31G* optimized structures for the ground-state carbon–oxygen attack are given in Figure 3a–f, and the corresponding energetic data are given in Table 1. Each of these structures in fact corresponds to the lowest energy solution of the CI problem in the MC-SCF, although, as we shall now discuss, the electronic configuration for diradicaloid minimum correlates diabatically with an n-π^* excited-state C–O and a ground-state C=C. Figure 3a shows the ground-state fragmentation transition state from the *gauche* minimum toward reactants with a carbon–oxygen bond distance of 1.60 Å (cf. 1.48 Å in oxetane). The electronic configuration of the attacking formaldehyde correlates with a mixture of the ground- and excited-state reactant configurations since the terminal methyl hydrogens are rotated by ca. 37° relative to the forming C–O bond. Thus the transition state arises, at least in part, from an avoided crossing. In fact in the *gauche* minimum structure (Figure 3b) where the C–O bond is essentially formed at 1.45 Å, the formaldehyde fragment is perpendicular to the ethylene suggesting that it correlates diabatically with the excited state and corresponds with VB structure **II** in Figure 1. The second *gauche* transition state is shown in Figure 3c. This is the transition state to ring closure to oxetane and although the radical centers are still highly separated at 2.74 Å there should be no further barrier to the coupling of the radical electrons to form the carbon–carbon bond. The torsional angle of the ethylenic and carbonyl fragment about the forming C–O bond has reduced from ca. 100° in the minimum and fragmentation transition state to 32° as the system ring closes to products. Again, from the angle of torsion of the CH_2, about the carbonyl C–O bond, this transition structure arises at least in part from an avoided crossing. The gauche minimum on the ground state therefore has an electronic configuration corresponding to diradical **II** of Figure 1. Thus the "excited-state

Table 1. Total and Relative Energies of Optimized Critical Points (CASSCF/6-31G* Six Electron/Five Orbitals)

structure	description	energy, Hartrees	rel E,[a] kcal mol^{-1}
	Reactants/Products		
Figure 2a	ethylene ground state	−78.060 26	
Figure 2b	ground-state formaldehyde	−113.901 56	
	vertically excited formaldehyde—n, π^*	−113.747 46	
Figure 2c	excited-state formaldehyde	−113.777 45	
Figure 2d	ground-state oxetane	−191.949 59	
	ground-state reactants	−191.961 82	
	excited-state reactants—n, π^*	−191.807 72	
	excited-state minmum—n, π^*	−191.837 71	
	C–O Attack		
Figure 3a	*gauche* fragmentation transition state (**I/II**)	−191.855 37	+1.9
Figure 3b	*gauche* diradical minimum (**II**)	−191.858 37	0.0
Figure 3c	rotational transition state to products	−191.854 10	+2.7
Figure 3d	*trans* fragmentation transition state (**I/II**)	−191.850 47	+5.0
Figure 3e	*trans* diradical minmum (**II**)	−191.858 75	−0.2
Figure 3f	rotational TS from *gauche* to *trans* minmum	−191.856 21	+1.4
Figure 4a	*gauche* conical intersection (**I/II**)	−191.816 23	
		−191.816 16[b]	+26.0
Figure 5a	*trans* conical intersection (**I/II**)	−191.818 27	
		−191.817 47[b]	+25.7
Figure 6	midpoint intersection geometry (**I/II**)	−191.796 68	
		−191.794 27[b]	+40.2
	C–C Attack		
Figure 7a	*gauche* fragmentation transition state	−191.871 18	+0.2
Figure 7b	*gauche* diradical minmum (**III**)	−191.871 46	0.0
Figure 7c	rotational transition state to products	−191.869 63	+1.15
Figure 7d	*trans* diradical minmum (**III**)	−191.874 63	+2.0
Figure 7e	rotational TS from *gauche* to *trans* minmum	−191.869 73	+1.1
Figure 8a	*gauche* conical intersection (**III/IV**)	−191.868 82	
		−191.868 71[b]	+1.7
Figure 9a	*trans* conical intersection (**III/IV**)	−191.869 54	
		−191.869 43[b]	+1.3
	Triplet		
Figure 10a	C–O *gauche* minmum (**II**)	−191.857 98	
Figure 10b/b′	C–C *gauche* minmum (**IV/III**)	−191.871 08/−191.869 12	
Figure 10c	C–O *trans* minmum (**II**)	−191.858 38	
Figure 10d	C–C *trans* minmum (**III**)	−191.868 79	

[a] The relative energies are calculated taking the *gauche* 1,4-diradical minmum as reference for the C–O and C–C mechanisms in turn. The relative energies in kcal mol^{-1} are then calculated for the remaining critical points on the reaction coordinate. [b] Calculated with state averaged CASSCF.

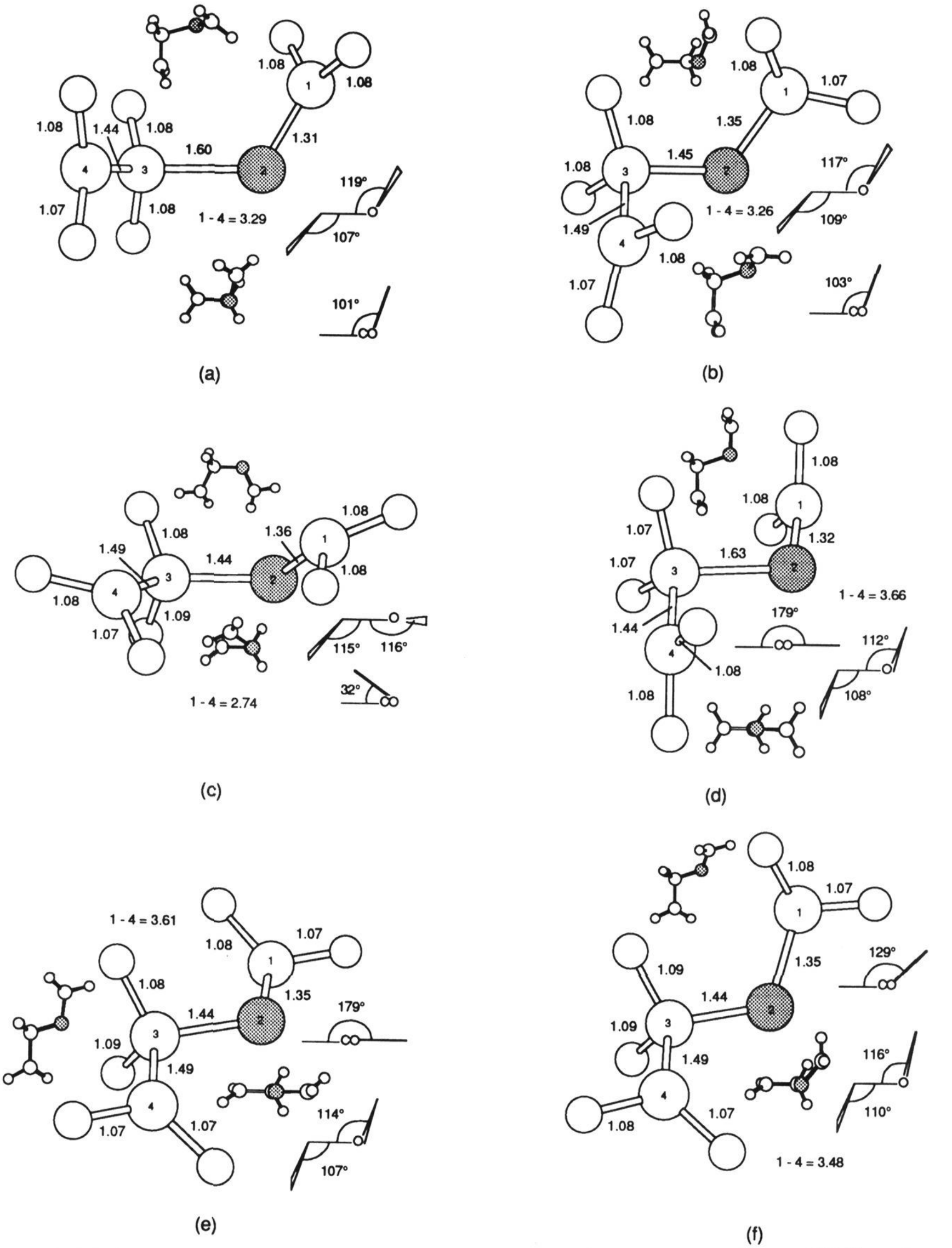

Figure 3. Optimized ground-state CASSCF/6-31G* geometries for C–O attack: (a) *gauche* fragmentation transition state **I/II**, (b) *gauche* 1,4-diradical minimum **II**, (c) rotational transition state to product, (d) *trans* fragmentation transition state **I/II**, (e) *trans* 1,4-diradical minimum **II**, and (f) transition state from *trans* minimum to *gauche* minimum.

configuration" **II** (from a diabatic point of view) must dip below the "ground-state configuration" **I** in the region of the *gauche* diradical minimum.

The structures corresponding to the carbon–oxygen *trans* reaction coordinate are detailed in Figure 3d–f. Critical points have been located for the fragmentation transition state (Figure 3d), minimum (Figure 3e) and transition state to the formation of the *gauche* minimum conformation of the diradical (Figure 3f). Electronically, the situation is only slightly different from the *gauche* pathway. The fragmentation transition state (Figure

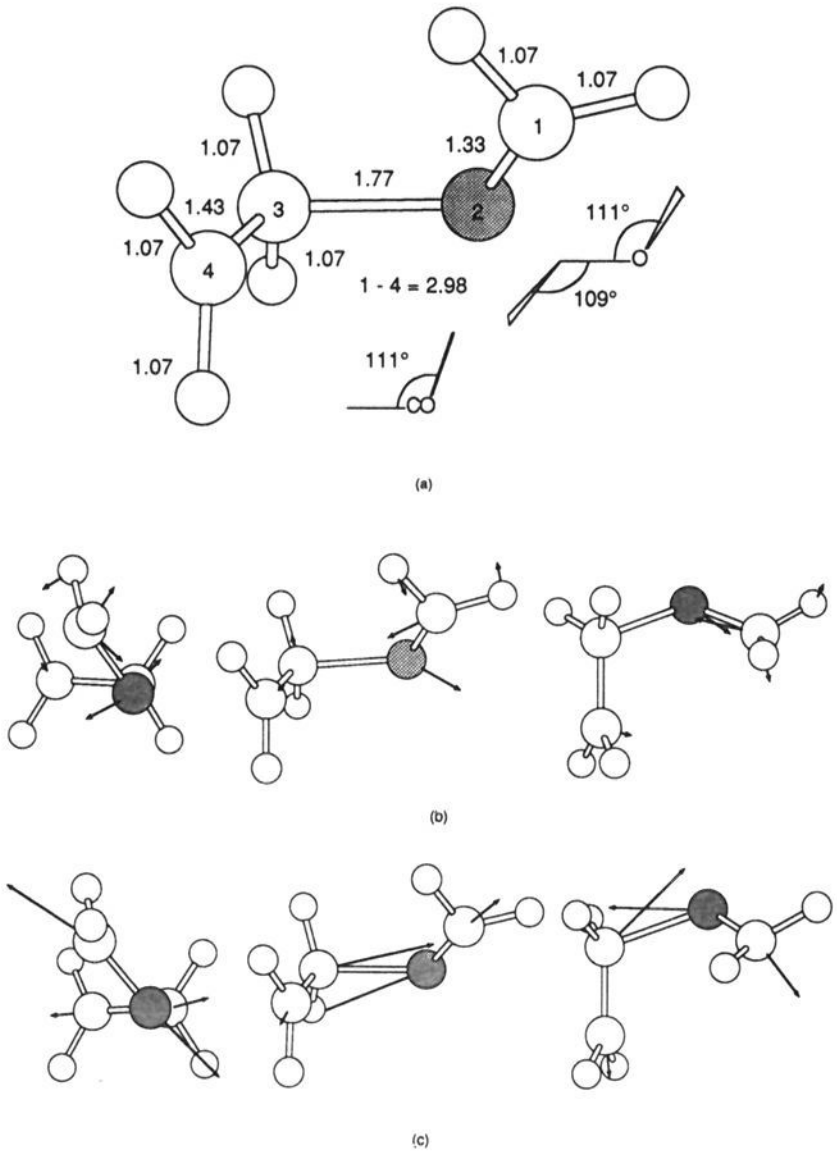

Figure 4. (a) State averaged CASSCF/6-31G* optimized geometry of C–O *gauche* conical intersection **I/II**, (b) side, perspective, and top views of calculated nonadiabatic coupling vector, $\langle\Psi_1|\partial\Psi_2/\partial q\rangle$, and (c) side, perspective, and top views of calculated gradient difference vector, $\partial(E_2-E_1)/\partial q$.

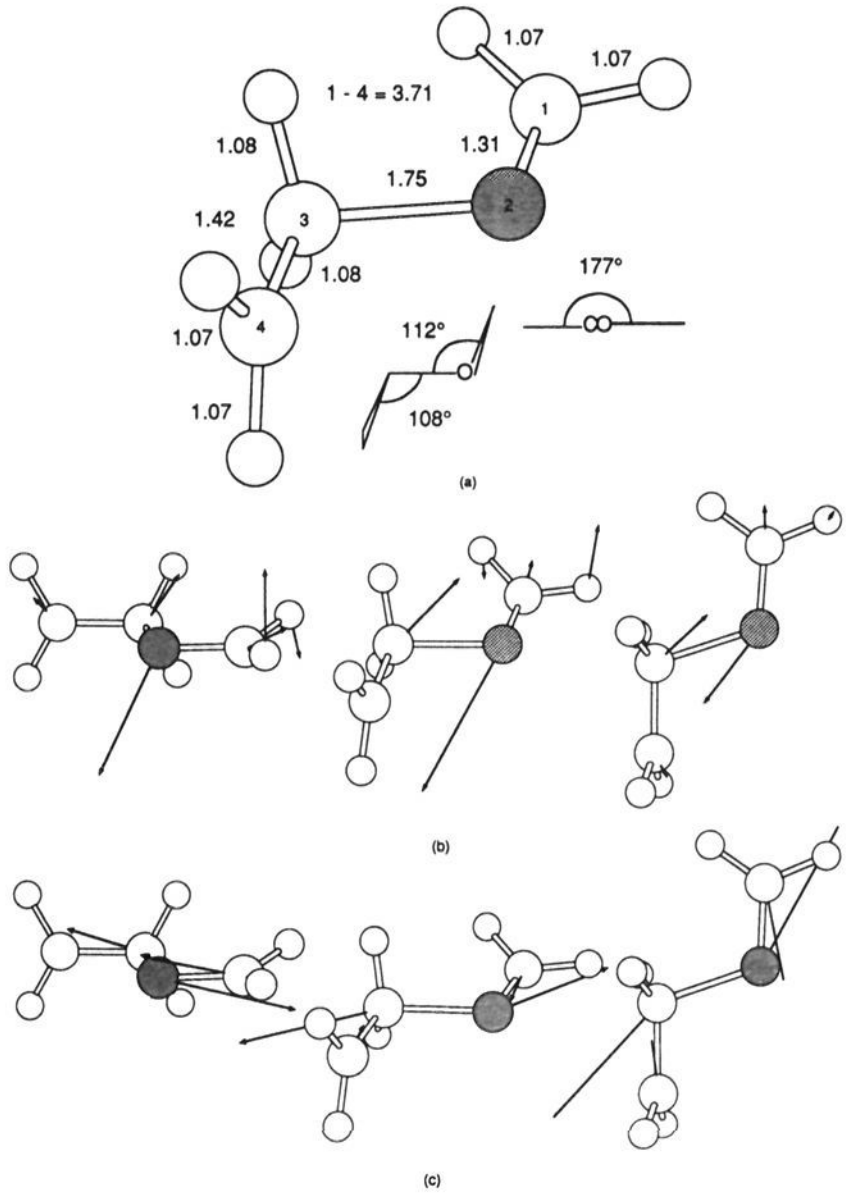

Figure 5. (a) State averaged CASSCF/6-31G* optimized geometry of C–O *trans* conical intersection **I/II** (b) side, perspective, and top views of calculated nonadiabatic coupling vector, $\langle\Psi_1|\partial\Psi_2/\partial q\rangle$, and (c) side, perspective, and top views of calculated gradient difference vector, $\partial(E_2-E_1)/\partial q$.

3d, C–O distance 1.63 Å) indicates the attack of the ground-state formaldehyde on the ethylene in a manner which may be described by VB structure **I** of Figure 1. By the time the *trans* minimum has been reached (Figure 3e, C–O distance 1.44 Å) a rotation of the carbonyl hydrogens has occurred and the diradical corresponds to VB structure **II** of Figure 1. In the transition state between the *trans* minimum and the *gauche* minimum shown in Figure 3f, (forming C–O distance 1.44 Å), the torsional angle between the ethylene and carbonyl has decreased from 179° to 129°. This structure could not be optimized accurately (RMS force 0.0008 au) because, in addition to the negative direction of curvature corresponding to rotation about the C–O bond, there is a near zero force constant for the rotation of the ethylenic terminal methylene. In general, the diradical region is extremely flat as is evident from the energetic data contained in Table 1. The barriers which do arise may be attributed to the slight steric changes as the system rotates around the forming carbon–oxygen bond.

The photochemical cycloaddition of alkene and carbonyl fragments is a nonadiabatic photochemical reaction. The *gauche* minimum on the ground state has an electronic configuration corresponding to diradical **II** of Figure 1 and thus correlates diabatically with an n-π^* excited-state C–O and a ground-state C=C. The fragmentation transition state from this minimum corresponds to an *avoided crossing*. However, in order for the nonadiabatic reaction to take place we must find the lowest energy S_1/S_0 conical intersection where the photoexcited system decays nonradiatively to S_0. The S_1/S_0 intersection space has been investigated along the carbon–oxygen reaction coordinate by locating three conical intersection points: *gauche* (Figure 4a), *trans* (Figure 5a), and *centrally bonded* (Figure 6). (The MC-SCF/6-31G* energies of the ground and excited states calculated with state averaged orbitals, required to correctly treat the

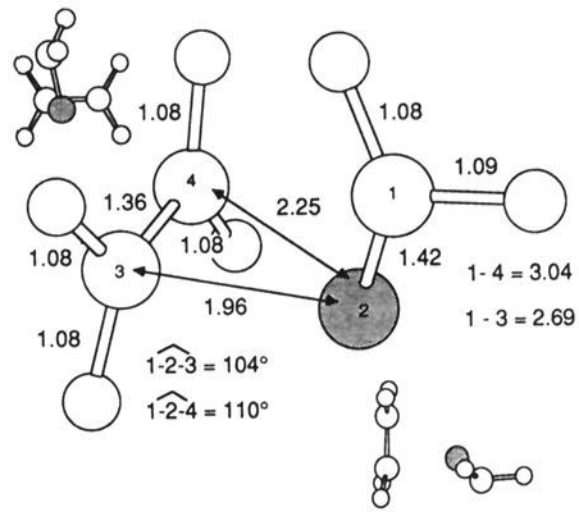

Figure 6. State averaged CASSCF/6-31G* geometry of C–O *centrally bonded* conical intersection.

degeneracy, are given in Table 1.) The *gauche* and *trans* structures have been fully optimized and therefore correspond to stable structures within the $n-2$ dimensional space of conical intersection points, where the ground and excited states are degenerate. The common features of these two structures are (i) the carbon–oxygen bond lengths, which are 1.77 and 1.75 Å respectively, and (ii) it is clearly an attack of an excited-state carbonyl (VB structure **II**) on the ground-state ethylene. The *centrally bonded* species (Figure 6) lies on the same space but does not correspond to a minimum. We give this point only to emphasize that the region of geometrical space over which the degeneracy (i.e., the intersection space) extends is rather large.

The origin of these conical intersections is easy to understand qualitatively. The ground- and excited-state correspond to simple changes in the configuration of electrons in the n/π system of the

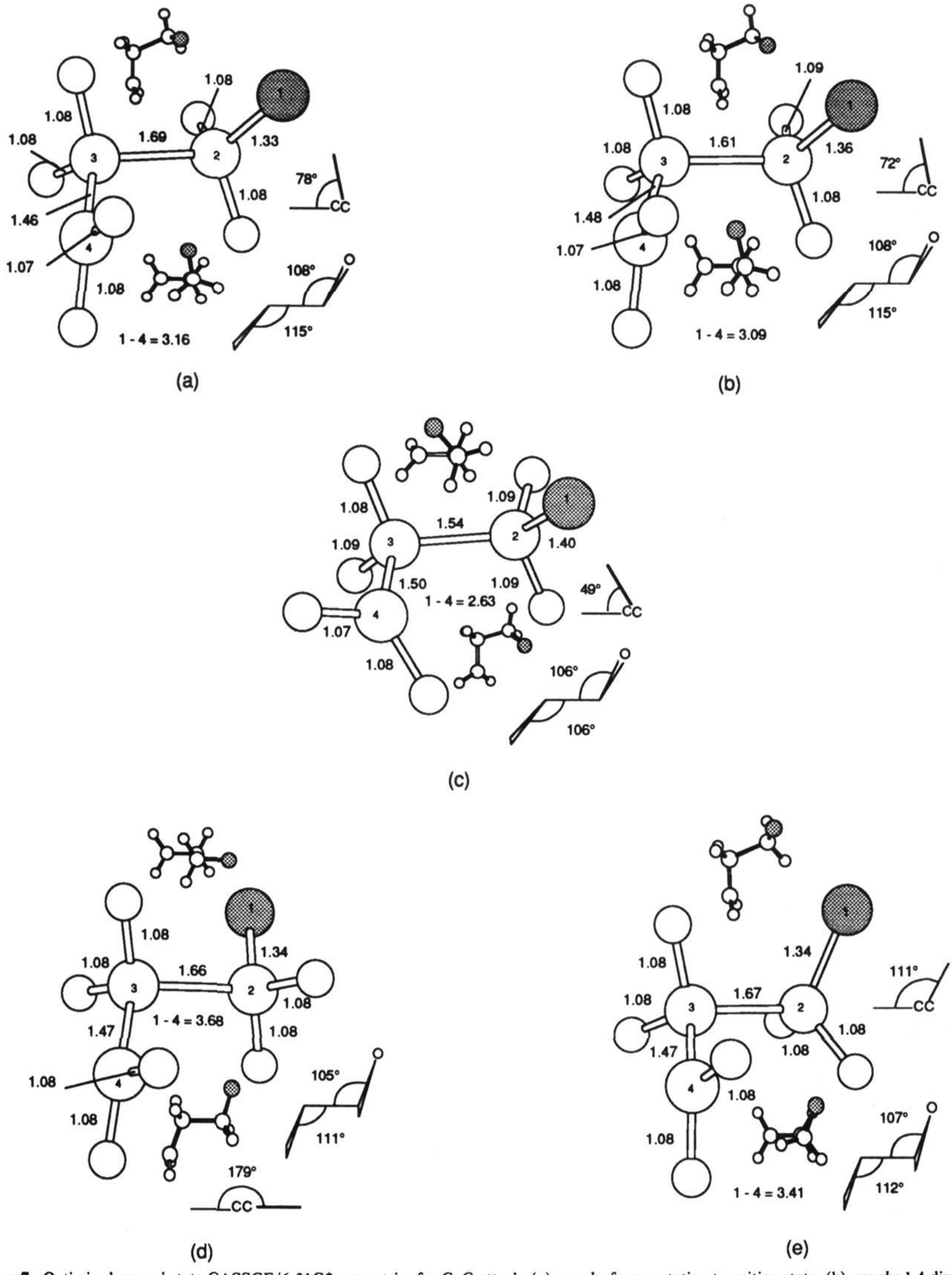

Figure 7. Optimized ground state CASSCF/6-31G* geometries for C–C attack, (a) *gauche* fragmentation transition state, (b) *gauche* 1,4-diradical minimum **III**, (c) rotational transition state to product, (d) *trans* 1,4-diradical minimum **III**, (e) transition state from *trans* minimum to *gauche* minimum.

carbonyl, represented by VB structures **I** and **II** (Figure 1), and the degeneracy occurs at a structure where the two configurations have the same energy. The critical factors which decide this are the forming carbon–oxygen bond length together with the orientation of the carbonyl moiety and the ethylenic C–C bond length together with the carbonyl C–O bond length. In the *gauche* conical intersection structure shown in Figure 4a the formaldehyde is perpendicular to the ethylene and the forming C–O bond length is 1.77 Å. The system in this way is in a situation where S_0 (VB structure **I**, Figure 1) and S_1 (VB structure **II**, Figure 1) configurations are energetically equivalent. Once this condition is satisfied the molecule may rotate around the carbon–oxygen bond without lifting the degeneracy although the energy will rise as the topology of the $n-2$ intersection space is experienced. The structure shown in Figure 6, where the formaldehyde is positioned in the middle of the ethylene, was located on the conical intersection although it is not a minimum in the $n-2$ space and is higher in energy than the *gauche* or *trans* conical intersection

structures. If a constrained optimization is started at this point on the intersection, the structure relaxes back to the *gauche* conical intersection minimum. The location of this point on the crossing surface further demonstrates the extent of geometry space into which the intersection is located. Thus it appears when the two fragments approach in the excited state along the necessary perpendicular path, once the critical forming C–O bond length is reached, the system can undergo a fully efficient decay to the ground state. From Table 1 one observes that the *gauche* conical intersection lies ca. 5.3 kcal mol^{-1} lower in energy than the vertical excitation energy from ground-state reactants. However, it is ca. 13.5 kcal mol^{-1} higher in energy than the relaxed excited-state reactant minimum.

The nature of the C–O conical intersection in terms of the geometric variables is most easily understood in terms of the nonadiabatic coupling and gradient difference vectors shown in Figure 4b,c and Figure 5b,c. They define the two-dimensional space (x_1x_2 plane in Scheme 2) yielding the double cone shape of the S_0/S_1 surfaces associated with the conical intersection point (i.e., the directions of movement which will lift the degeneracy). The calculated nonadiabatic coupling vector and gradient difference vector for the *gauche* C–O conical intersection are shown in Figure 4, parts b and c, respectively. The nonadiabatic coupling vector is dominated by a motion leading to the contraction of the carbonyl bond, whereas the gradient difference vector involves a similar motion in the forming C–O bond. It is obvious that these two motions will lead to lifting of the degeneracy if the nature of the intersecting states is considered in terms of the VB structures **I** and **II**. Shortening of the formaldehyde C–O bond will result in the stabilization of the ground-state configuration (VB structure **I**) and the destabilization of the excited-state configuration (VB structure **II**). Similarly the shortening of the forming C–O bond along the gradient difference vector will result in a raising of the energy of the ground-state configuration (VB structure **I**) and a lowering of the energy of the excited-state configuration (VB structure **II**). The nonadiabatic coupling and gradient difference vectors calculated for the *trans* C–O conical intersection minimum are shown in Figure 5, parts b and c, respectively.

II. Singlet Carbon–Carbon Reaction Path. The second possible mode of attack of the carbonyl on the ethylene corresponds to the formation of a C–C bond and 1,4-diradical (Scheme 1, **1** + **2** → **3b** → **4**). The structures located on the ground-state potential surface for the C–C attack are illustrated in Figure 7a–e. From the energetic information contained in Table 1 it can be seen that the surface in this region is extremely flat. The *gauche* fragmentation transition state, shown in Figure 7a, has a C–C bond length of 1.69 Å which becomes 1.61 Å at the *gauche* minimum of Figure 7b. The radical centers are well-separated at 3.09 Å suggesting little interaction between them. Figure 7c shows the transition state for ring closure from the *gauche* diradical structure. In this structure the C–C bond is completely formed at 1.54 Å, and the torsional angle about the C–C bond has closed to 49°. The distance between the radical centers is 2.63 Å suggesting a weak interaction of the unpaired electrons. Similarly, the *trans* family of critical points are shown in Figure 7d,e. There were problems experienced in the optimization of some of the structures on the *trans* reaction path due to (a) the very flat nature of the potential surface in this region and (b) the near degeneracy of the potential energy surfaces of ground and excited state. The latter problem arises because the radical centers are so widely separated, ca. 3.7 Å in the *trans* minimum, and there is thus little energetic difference between the two electronic configurations at the oxygen (**III** and **IV** of Figure 1). Indeed despite exhaustive attempts, the *trans* minimum structure (Figure 7d) could not be optimized with a maximum force lower than 0.002 au (RMS force 0.0005 au). For a similar reason, the transition state between the *trans* transition state and the *gauche* diradicaloid minimum (Figure 7e) was obtained only with a maximum force of 0.002 au (RMS force 0.0009 au). Finally, the

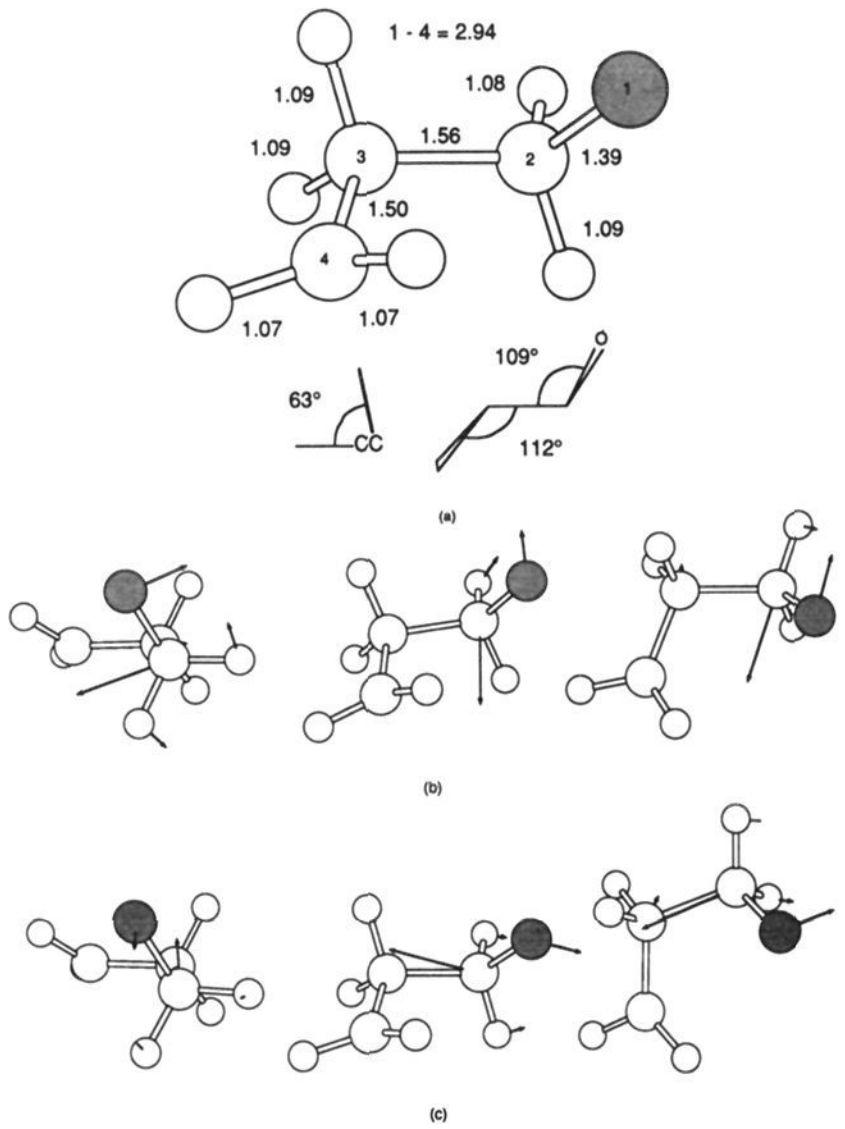

Figure 8. (a) State averaged CASSCF/6-31G* optimized geometry of C–C *gauche* conical intersection **III**/**IV**, (b) side, perspective and top views of calculated nonadiabatic coupling vector, $\langle\Psi_1|\partial\Psi_2/\partial q\rangle$, and (c) side, perspective and top views of calculated gradient difference vector, $\partial(E_2 - E_1)/\partial q$.

trans fragmentation transition state could not be obtained at the 6-31G* level since the geometry optimization always relaxed to the minimum structure.

Thus the ground-state reaction path for the diradical C–C attack is exceedingly flat with minima and transition states located in an energy range of only a few kcal mol^{-1}. Further, the ground and excited states are very close in energy everywhere because they differ only in the electronic configuration at the oxygen. Nevertheless, inspection of the MC-SCF results reveals, unambiguously, that all of these ground-state critical points (Figure 7) lie on a surface that correlates with VB structure **III**. We now turn our attention to the excited state. From the preceding discussion, it is apparent that the surface that correlates with VB structure **IV** must dip only slightly below the ground-state reaction path at geometries which are not very different to those optimized on the ground-state reaction path (Figure 7). The conical intersection geometries where S_1 to S_0 decay occurs for the C–C reaction path are shown in Figure 8a and Figure 9a. Note that the C–C bond (1.56 Å) is completely formed at the conical intersection geometry. Thus the two electrons of the original π-bond in formaldehyde are completely decoupled and a degenerate radical center is created on the oxygen of the formaldehyde and C_4-carbon of the ethylene. The energy of this conical intersection lies some 38 kcal mol^{-1} below the energy of the vertically excited reactants but only approximately 6.5 kcal mol^{-1} below the *gauche* diradical minimum for C–O attack. Projections of the nonadiabatic coupling and gradient difference vectors which define the directions where the degeneracy is lifted (i.e., the double-cone shape) at the conical intersection are shown for the *gauche* and *trans* structures in Figures 8b,c and 9b,c, respectively. For both the *gauche* and *trans* structures the nonadiabatic coupling and gradient difference involve rotation about, and shortening of, the forming C–C bond accompanied by changing of the formaldehyde C–O bond length.

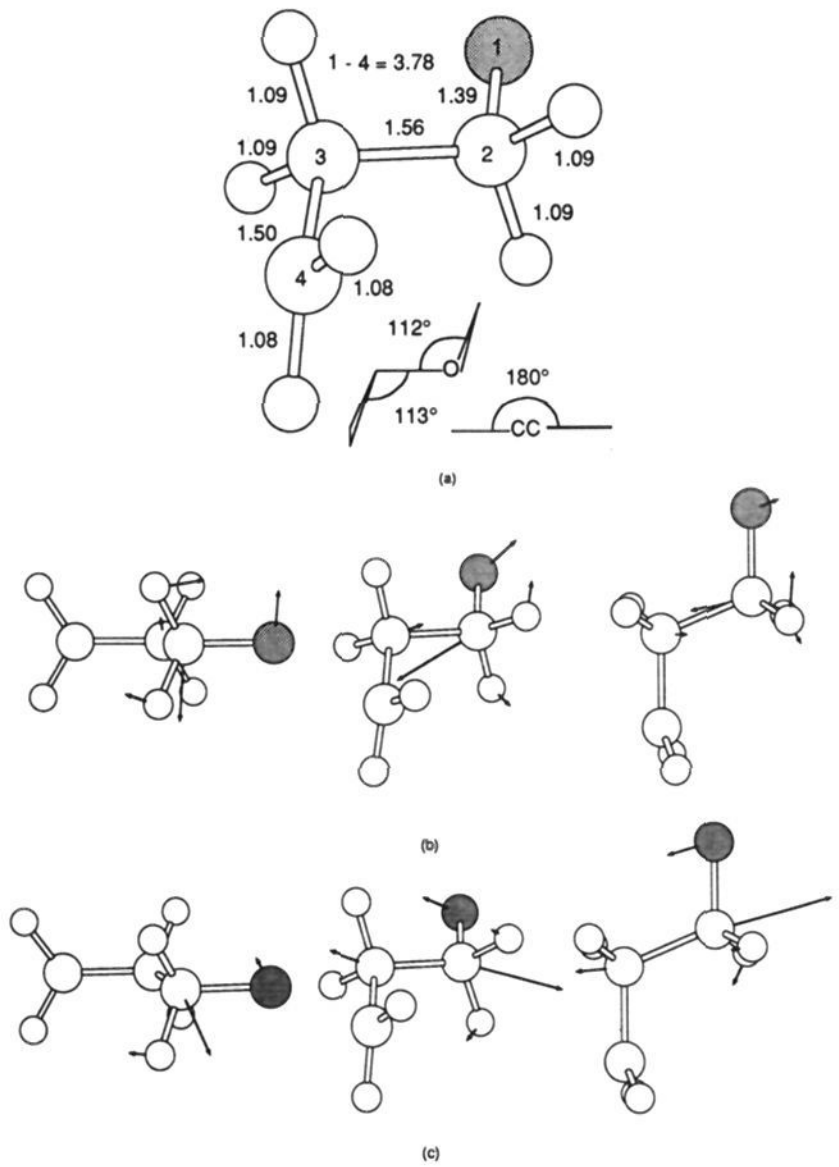

Figure 9. (a) State averaged CASSCF/6-31G* optimized geometry of C–C *trans* conical intersection **III**/**IV**, (b) side, perspective, and top views of calculated nonadiabatic coupling vector, $\langle \Psi_1/\partial\Psi_2/\partial q \rangle$, and (c) side, perspective, and top views of calculated gradient difference vector, $\partial(E_2-E_1)/\partial q$.

The behavior of the excited-state surface (i.e., VB structure **IV**) in the region of the conical intersection is unusual. The gradient of the excited state is very small in all geometrical parameters at the optimized conical intersection geometry. This suggests that the excited state has a real minimum in this region (i.e., not a conical point) and that the conical intersection point can be seen as a very weakly avoided crossing rather then a true conical intersection. While it is impossible to do a meaningful optimization of such an excited-state minimum because the states are degenerate, this conjecture is supported by the fact that the optimized structure for the triplet diradical minimum (which we will discuss subsequently) corresponding to VB structure **IV** has a structure (and an energy) virtually identical to the optimized conical intersection geometry shown in Figure 8. Thus the region of S_1 to S_0 decay for the C–C attack occurs near the products where the surface of the diradical structure **IV** dips only slightly below the ground-state surface in the region of an excited-state minimum.

Thus the nature of the singlet reaction paths for the photochemical reaction that originates from n-π^* formaldehyde differs substantially for C–O and C–C attack. For CO attack, the ground-state diradicaloid minimum corresponds to VB structure **II** which correlates diabatically with an n-π^* excited state C–O and a ground-state C=C, and there is a conical intersection at a forming C–O bond length of 1.77 Å. For C–C attack, the ground-state diradicaloid minimum corresponds to the VB structure **III**. The excited-state surface corresponding to VB structure **IV** appears to have its minimum in the region of a conical intersection with the forming C–C bond length of 1.56 Å. Thus for C–C attack, the photochemical reaction will be quasi-concerted because the surface hop to the ground-state surface occurs close to the products (i.e., after the ground-state diradical minimum). In contrast, for C–O attack, the photochemical reaction will be nonconcerted. The surface hop occurs before the ground-state diradical which is "protected" by low-energy transition states to fragmentation and ring closure.

III. Triplet (n,π^*) Potential Surface. The formation of oxetanes is found to occur readily from T_1 for reaction of electron rich alkenes and is assumed to occur via C–O bond formation. Apparently the triplet reaction (assumed to occur via C–C bond formation) does not occur for electron poor alkenes. Obviously, the mechanistic aspects for a triplet reaction which involves a diradicaloid intermediate should be very similar to the singlet provided the diradical centers are decoupled (i.e., at a large distance). The excited-state branch of the reaction coordinate must terminate at the "excited-state" diradicaloid minima correspond to VB structures **II** for C–O attack or **IV** for C–C attack. The ground-state branch of the reaction must continue from this point after intersystem crossing. Thus our objective in this section is merely to discuss the nature of these triplet diradicaloid minima. Experimentally, the triplet 1,4-diradical species has been detected spectroscopically in the reaction of benzophenone and 1,4-dioxene.[26] Formation of the spin protected diradical in this reaction has long been proposed as the reason for the lack of stereoselectivity resulting from bond rotations which may occur within the lifetime of the diradical.

We have characterized the *gauche* and *trans* conformers that correspond to VB structures **II** and **IV** on the triplet surface, and the structures are shown in Figure 10a–d with corresponding MC-SCF/6-31G* energies in Table 1. Further, the structure of the triplet diradical minimum corresponding to VB structure **III** has been obtained. The geometry and energy are essentially identical to those of VB structure **IV**, and the structure is indicated in brackets in Figure 10b′. Since the diradical centers in all these structures are well-separated, there is a close correspondence with the singlet results. We now briefly summarize the implications for C–O versus C–C attack.

For C–O attack, the geometry that corresponds to VB structure **II**, the *gauche* 1,4-diradicaloid on the carbon–oxygen reaction path, is shown in Figure 10a. The C–O bond is completely formed in this structure (1.45 Å) and the formaldehyde C–O π-bond broken (1.35 Å). Both the geometry and the energy are almost identical with the singlet *gauche* diradicaloid (Figure 3b). The geometry of the triplet structure has a torsional angle about the forming C–O bond of 77° compared with 103° in the singlet ground state *gauche* minimum. The CASSCF/6-31G* energy of the singlet ground state was recalculated at the triplet minimum geometry and is only 0.8 kcal mol^{-1} higher in energy than the triplet. The situation is similar for *trans* C–O bonded structures.

The situation is rather different for C–C attack. The geometrical parameters of the two (essentially degenerate) carbon–carbon *gauche* triplet minima (VB structures **III** and **IV**) are shown in Figure 10b/b′, and the energies are listed in Table 1. The energies and optimized geometries of the two C–C bonded triplet diradicals are almost identical to the singlet C–C gauche conical intersection geometry shown in Figure 8a. Thus, not only is the triplet diradical degenerate with singlet diradical corresponding to VB structure **IV** as in the C–O triplet minimum but also it lies at the point of the conical intersection of the ground and first excited singlet states. Therefore at this point four states are essentially degenerate, two singlets and the two triplets. From the arguments presented in the discussion of the C–C singlet reaction it is not surprising that the triplet minima coincide with the singlet conical intersection: the carbon–carbon bond has been fully formed at 1.57 Å and the formaldehyde carbon–oxygen bond broken at 1.39 Å and the two radical centers are decoupled at a distance of 2.93 Å. Again, similar arguments apply to the *trans* region. Note, that because of the degeneracy of the two C–C bonded triplets it is not possible to confirm the nature of these minima by a frequency computation.

In summary, the minima of the triplet surface that correlate with n-π^* excited formaldehyde (VB structures **II** and **IV**) coincide with the corresponding singlet structures (a diradicaloid minimum

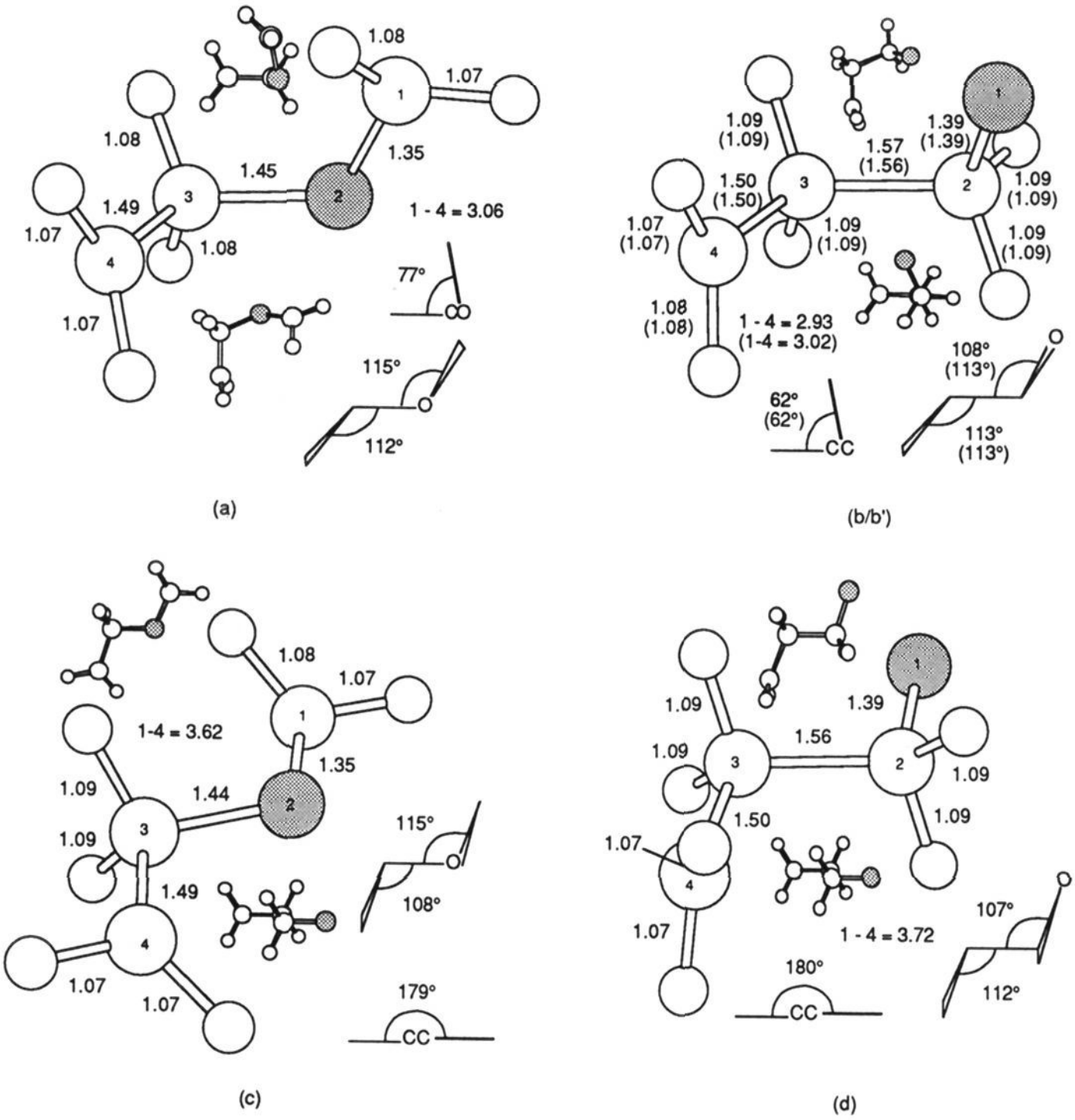

Figure 10. CASSCF/6-31G* optimized geometries for (a) C–O *gauche* triplet minimum **II**, (b) C–C triplet *gauche* minima (parameters shown correspond to VB structure **IV** those in parentheses correspond to VB structure **III**), (c) C–O *trans* triplet minimum **II**, and (d) C–C *trans* triplet minimum **III**.

for C–O attack and a conical intersection for C–C attack). Since singlet and triplet energies are essentially equal at these geometries, the efficiency of the triplet reaction must be controlled by the nature of the spin-orbit coupling matrix element.

4. Conclusions

Our purpose in the paper is to present computations for a model system and thus provide a general basis for future mechanistic discussion and the rationalization of experimental work. While, in conjugated ketones there is rapid intersystem crossing to the triplet state, the singlet mechanism has been firmly established for aliphatic certain ketones.[8] Thus both singlet and triplet mechanisms presented in this work can provide useful models. Turro[4] rationalizes his quenching experiments for electron poor versus electron rich ethylenes on the basis of a face to face (C–C) or face to edge (C–O) attack. Thus while the C–O attack is often used to understand the mechanism, the C–C mechanism does merit serious consideration.

In order to summarize the mechanistic implications of the results that we have just presented, it is helpful to present the surfaces for the C–O and C–C mechanisms in a schematic way as illustrated by Schemes 3 and 4, respectively. These "pictures" are designed to convey only the general topological relationships between the various minima, transition states and surface crossings. A reference to the figure containing the optimum geometries is shown where appropriate. It has been "artistically convenient" to exaggerate the depth of the various minima. In fact, the energies given in Table 1 indicate that the surfaces are very flat. Only the potential surfaces for the *gauche* pathway are represented in each case as these may be viewed as the most important reaction path from reactants to products. The *trans* pathway merely represents an indirect route to the *gauche* region of the potential surface.

We begin with a discussion of the schematic surface for the carbon–oxygen attack shown in Scheme 3. The labels FF and FE on the states serve to remind us of the geometric structures of the diradical intermediates: "face-to-face" from the ground-state formaldehyde (resulting in the formation of the 1,4-diradical with the VB structure **I**) and "face-to-edge" from attack of the excited-state formaldehyde (resulting in the formation of the 1,4-diradical with the VB structure **II**). The diradical minimum region of the surface correlates with VB structure **II** and spans a fragmentation transition state (TS1), minimum and rotational transition state (TS2) to ring closure, all separated by less than 3 kcal mol^{-1}. The fragmentation transition state (TS1) lies 66.8 kcal mol^{-1} above the ground-state reactants. Since the diradical minimum correlates diabatically (VB structure **II**) with n-π^* excited formaldehyde, the transition state TS2 corresponds to an avoided crossing. For the singlet photochemical reaction the important feature is the decay point corresponding to the conical intersection (C.I. in Scheme 3). This conical intersection lies ca. 5.3 kcal mol^{-1} lower in energy than the vertical excitation from reactants and occurs early along the reaction coordinate with the optimized structure possessing a forming C–O bond length of

Scheme 3

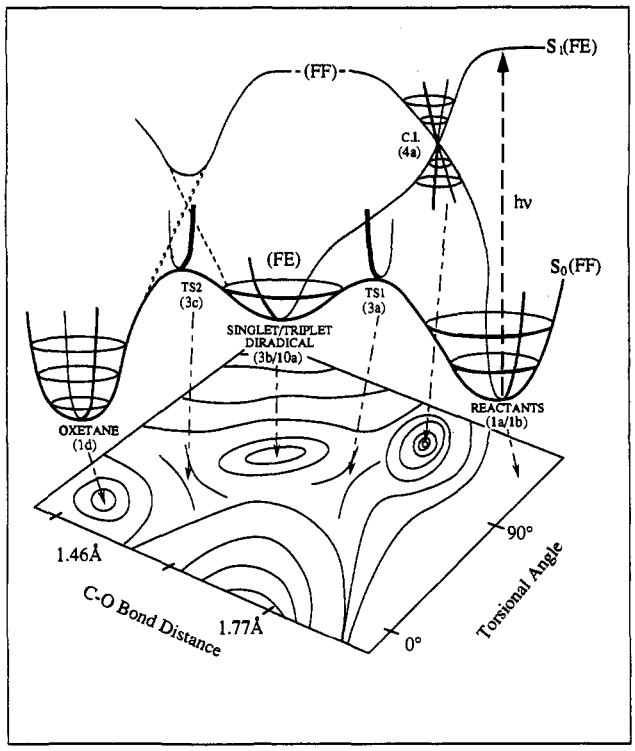

Scheme 4

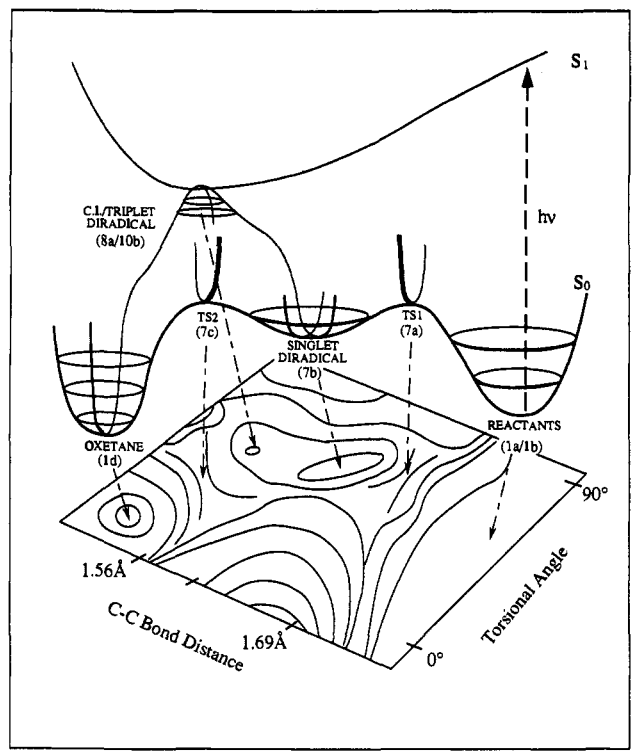

1.77 Å. (In fact the conical intersection lies some 13.5 kcal mol^{-1} higher than the energy of the relaxed geometry of the excited-state reactants. Scheme 3 does not include this feature.) The singlet and triplet diradical minima are essentially coincident, and the nature of the spin-orbit coupling must control the efficiency of the triplet reaction. Thus the C–O attack for the model Paterno–Buchi reaction is *non-concerted*. The first step in the reaction involves the formation of a diradical intermediate (or fragmentation back to the reactants) either directly in the case of the triplet or via a fully efficient decay process involving a conical intersection in the case of the singlet. The second step involves the closure of this diradical over a small barrier. The fast rate of diradical formation is explained by the rapid passage through the conical intersection. This process takes place on the time scale of one vibrational period.[22]

We now turn to a discussion of schematic surface for the carbon–carbon attack mechanism shown in Scheme 4. In general, the diradical region corresponding to the C–C attack lies ca. 10 kcal mol^{-1} *lower* in energy than the C–O region. In contrast to the C–O attack, the diradicaloid region of the ground-state surface correlates with ground-state reactants (i.e., VB structure **III**). However, it is very flat and spans a minimum, a fragmentation transition state and rotational transition state all separated by ca. 1.0 kcal mol^{-1}. The fragmentation transition state lies 56.8 kcal mol^{-1} above the ground-state reactants. The diradicaloid corresponding to VB structure IV which correlates with n-π^* excited formaldehyde has a C–C bond length of 1.56 Å and corresponds to the conical intersection geometry, in the case of the singlet, and to a true minimum (where VB structures **III** and **IV** are degenerate) in the case of the triplet. Thus for the singlet photochemistry the decay to S_0 occurs close to the products. Thus the nonadiabatic reaction path from the excited-state reactants passes via the conical intersection, where the C–C distance is 1.56 Å, and the energy is only 1.6 kcal mol^{-1} above the triplet diradical minimum, directly to products. Since the surface hop via the conical intersection will be fully efficient, the reaction appears to be *concerted*. However, a certain fraction of photo-excited reactant can evolve via a nonconcerted route since the formation of the C–C singlet diradical is also possible from the same conical intersection. Again, the efficiency of the triplet reaction, which must proceed via the same path, will be controlled by the nature of the spin-orbit coupling interaction.

For the singlet reaction there are two pathways a *nonconcerted* C–O attack and a *concerted* C–C attack. Thus the overall nature of the nonadiabatic reaction path is determined by whether the system decays early (via C–O) attack or late via C–C attack. Because of this fact, the stereochemistry and the efficiency of the "real" reaction will depend upon which excited-state reaction path is actually followed in the real system. This in turn is traditionally expected to be controlled mainly by the stability of the diradical that would correlate diabatically with the excited state reactants (the most stable diradical rule). However, our results indicate that this reasoning is incorrect! For the singlet reaction the two topological features of the excited-state surface that will control the course of the reaction are the conical intersections where one has fully efficient decay to the ground state. Thus it is the nature of the excited-state path that leads to the conical intersections that plays the decisive role in the mechanism. For C–C attack the conical intersection is essentially the same as the diradicaloid minimum (VB structure **IV**). However, for C–O attack, the conical intersection occurs early in the excited-state reaction path (C–O distance 1.77 Å) before the diradicaloid structure (VB structure **II**) that is actually on the lowest energy surface. In our computations, the conical intersection for the C–O attack occurs just below (5.3 kcal mol^{-1}) the energy of vertical excitation of the reactants and some 33 kcal mol^{-1} higher in energy than the conical intersection that occurs on the C–C attack which lies in a much lower energy region some 38 kcal mol^{-1} below the energy of vertical excitation of the reactants. Thus for the model reaction the concerted C–C mechanism is favored. The most stable diradical rule will not make such strong prediction. The diradicaloid for excited-state C–C attack, corresponding to VB structure **IV** (actually the conical intersection geometry of Figure 8a) lies just 6.5 kcal mol^{-1} below the *gauche* diradicaloid for excited state C–O attack corresponding to VB structure **II** (Figure 3b).

The prediction for the triplet cannot be formulated with the same level of certainty. In this case, the excited-state reaction path terminates at the diradical minima. For C–O attack, the triplet surface must still cross the singlet to reach the diradicaloid minimum corresponding to VB structure **II**. However, since the

spin-orbit coupling is many orders of magnitude smaller than the electronic interactions, the singlet and triplet surfaces will not interact and so can cross freely along the excited-state reaction coordinate leading to the diradical minimum. At the diradical minimum, the singlet and triplet surfaces are degenerate, and the system will presumably oscillate many times before intersystem crossing takes place. (As pointed out this triplet diradical has been detected experimentally[26].) For C–C attack, the triplet diradical minimum is located at the same geometry as the conical intersection between the two singlet states, and the efficiency of intersystem crossing will be determined by the nature of the spin-orbit coupling. Thus for the triplet, the reaction path can be predicted by the most stable diradical rule.

Experimentally, the detailed course of the reaction appears to depend critically on the nature of the reactants. Lack of stereoselectivity, regioselectivity, and violation of the most stable diradical rule which often occurs would appear to indicate C–O attack rather than the concerted C–C approach. The general inefficiency of the reaction as far as quantum yields are due to the extremely flat nature of the ground-state diradical region with a negligible barrier to fragmentation. This will be particularly true for the C–O attack, where the system decays directly to the diradicaloid.

Acknowledgment. This research has been supported by the SERC (UK) under grant Number GR/G 03335. Ian Palmer is grateful to the SERC (UK) for the award of a studentship. The authors are also grateful to IBM for support under a Joint Study Agreement. All computations were run on an IBM RS/6000.

Note added in proof: An exiplex (excited-state dimer) with a large interfragment distance, has been postulated for the Paterno Buchi reaction although direct experimental evidence is lacking. Recently Bonacic-Koutecky (Frie Universitat Berlin) and coworkers have optimized (unpublished, private communication) such exiplex minima with energies slightly lower than the conical intersections.